INTEGRATIVE PHYSIOLOGY

Central and peripheral mechanisms underlying respiratory deficits in a mouse model of accelerated senescence

Alembert Lino-Alvarado[1] · Octavio A. C. Maia[2] · Maria Aparecida Oliveira[3] · Ana C. Takakura[3] · Wothan Tavares-Lima[3] · Henrique T. Moriya[1] · Thiago S. Moreira[2]

Abstract

Aging invariably decreases sensory and motor stimuli and affects several neuronal systems and their connectivity to key brain regions, including those involved in breathing. Nevertheless, further investigation is needed to fully comprehend the link between senescence and respiratory function. Here, we investigate whether a mouse model of accelerated senescence could develop central and peripheral respiratory abnormalities. Adult male Senescence Accelerated Mouse Prone 8 (SAMP8) and the control SAMR1 mice (10 months old) were used. Ventilatory parameters were assessed by whole-body plethysmography, and measurements of respiratory input impedance were performed. SAMP8 mice exhibited a reduction in the density of neurokinin-1 receptor immunoreactivity in the entire ventral respiratory column. Physiological experiments showed that SAMP8 mice exhibited a decreased tachypneic response to hypoxia (FiO2 = 0.08; 10 min) or hypercapnia (FiCO2 = 0.07; 10 min). Additionally, the ventilatory response to hypercapnia increased further due to higher tidal volume. Measurements of respiratory mechanics in SAMP8 mice showed decreased static compliance (Cstat), inspiratory capacity (IC), resistance (Rn), and elastance (H) at different ages (3, 6, and 10 months old). SAMP8 mice also have a decrease in contractile response to methacholine compared to SAMR1. In conclusion, our findings indicate that SAMP8 mice display a loss of the NK1-expressing neurons in the respiratory brainstem centers, along with impairments in both central and peripheral respiratory mechanisms. These observations suggest a potential impact on breathing in a senescence animal model.

Keywords Breathing · Chemosensitivity · Dementia · Hypercapnia

Introduction

Life expectancy has consistently increased over the years, raising concerns among scientists and public health experts about the implications of an aging population. Statistical data indicate a significant rise in the number of individuals aged 60 and above, projected to grow from 900 million in 2017 to nearly 2 billion by 2050 [10]. Although aging is a natural, progressive, and irreversible part of the life cycle, it can lead to the development of chronic diseases and disabilities during senescence, such as cardiovascular diseases, Alzheimer's disease (AD), cancer, and others, which affect the body in physiological, environmental, psychological, behavioral, and social ways, reducing quality of life.

During the process of aging, patients often exhibit altered breathing patterns, such as irregularities in eupneic (normal) breathing and abnormal ventilatory responses to hypoxic (low oxygen) and hypercapnic (high carbon dioxide) conditions [22, 51]. These changes can result in reduced respiratory efficiency and increased susceptibility to respiratory illnesses such as pneumonia and sleep disordered breathing [36, 37], impacting both the quality of life and overall health of affected individuals. For example, hypoxia seems to be related to the normal aging and early AD-associated cognition and memory impairment [36]. However, further

Alembert Lino-Alvarado and Octavio A. C. Maia are considered first author and contribute equally.

✉ Thiago S. Moreira
tmoreira@icb.usp.br

[1] Biomedical Engineering Laboratory, University of Sao Paulo, Sao Paulo, SP, Brazil

[2] Department of Physiology and Biophysics, Institute of Biomedical Science, University of Sao Paulo, Sao Paulo, SP, Brazil

[3] Deptartment of Pharmacology, Institute of Biomedical Science, University of Sao Paulo, Sao Paulo, SP, Brazil

investigation is needed to fully comprehend the changes in both central and peripheral mechanisms of the respiratory physiology in aging.

The use of animal models, including mice, rats, fruit fly, and roundworms, has provided valuable insights into the aging-associated disorders. Various transgenic mice present accelerated aging and/or reduced lifespan and have been used to study the underlying mechanisms of physiology dysfunction during the aging process [12, 34, 52], such as changes in the autonomic, sensory, and motor regulation [41]. However, those results should be carefully interpreted, since the typical aging features are related to a single gene defect, which also promotes features not seen in wild old mice [19]. In this way, the Senescence Accelerated Mouse Prone 8 (SAMP8), which was established through phenotypic selection from a common genetic pool of AKR/J mice, has an advantage since the aging features occur due to a range of spontaneous mutation, closing to the normal aging [12, 46].

The aging features shown by SAMP8 mice are not restricted to reduced lifespan or a single aging-associated change, but include changes associated with AD, such as down-regulation in the expression of anti-aging factors [20, 22], glial degeneration [38], Aβ deposition [33], increases in oxidative stress [42], memory deficiency [26], cardiac dysfunction [41], renal damage [54], and hearing loss [24]. However, there is currently limited research available regarding the specific differences in the peripheral and central respiratory mechanisms of SAMP8 mice. In summary, studying the physiology of respiration during aging is crucial for understanding the full impact of these conditions on health. The SAMP8 mouse model offers unique insights into how senescence-related pathology affects the respiratory control, providing a valuable framework for developing therapeutic strategies aimed at mitigating respiratory impairments in patients. This study leverages the SAMP8 model to further explore these interactions, aiming to uncover new targets for intervention and improve the management of respiratory symptoms during the development of aging.

Material and methods

Animals

All animal procedures and protocols were approved and performed in accordance with the Guide for the Care and the Use of Laboratory Animals and approved by the Ethical Committee of the Institute of Biomedical Sciences of the University of São Paulo (CEUA#6,155,190,718). Inbreed SAMP8 and SAMR1 strains were derived from selective breeding of AKR/J mice, which showed early senescence and aging processes considered normal, respectively [44].

SAMP8 mice present spontaneous mutations resulting in a shorter lifespan, early learning and memory deficits, and reduced anxiety compared to age matched SAMR1 mice [30]. Dr. Dantas from the Institut d'Investigacions Biomèdiques August Pi i Sunyer (IDIBAPS), Barcelona, Spain, kindly donated the breeder SAMP8 and SAMR1 mice. For the present study, the animals were obtained by brother-sister mating and were kept in the vivarium of the Pharmacology Department in standard plastic cages at a constant temperature of 22ºC and submitted to a 12 h/12 h light/dark cycle with free access to standard food and water. Respiratory physiology (mechanics, hypoxia (HVR) or hypercapnia ventilatory response (HCVR)) and neuro-anatomical studies were conducted in 10-month-old male SAMP8 (N = 16) and SAMR1 mice (N = 17). The screening of respiratory mechanics over time was done in 3 (N = 12), 6 (N = 15) and 10-month-old SAMP8 (N = 16) mice.

Body weight and nasoanal length

All animals were weighed on the day of the experiment and the data were expressed in grams (g). After anesthesia, the nasoanal length, expressed in centimeter (cm), was evaluated, which corresponds to the measurement made from the snout to the anus of the animal.

Assessment of respiratory mechanics

Different groups of animals were employed to assess respiratory mechanics at each time point because of the invasiveness of the protocol. The protocol is detailed as follows. The animals were anesthetized with an intraperitoneal injection of ketamine (120 mg/kg, Syntec, Brazil) and xylazine (12 mg/kg, Ceva, Brazil). The trachea was cannulated with a custom-made 18G metallic cannula (BD, Brazil) and the jugular vein was cannulated for later injection of acetyl-β-methyl-choline chloride (methacholine-MCh, Sigma-Aldrich, USA), a muscarinic agonist. Mice were artificially ventilated with a positive end-expiratory pressure (PEEP) of 3 cmH$_2$O, at frequency of 150 breaths/min and a displaced volume of 10 mL/kg, using a small animal ventilator (flexiVent, SCIREQ, Canada). The neuromuscular blockade was made by intraperitoneal injection of pancuronium bromide (1 mg/kg, Cristália, Brazil). After seven minutes, a six-second recruitment maneuver (pressure ramp until 30 cmH$_2$O over 3 s followed by a 3 s end-inspiratory pause) was carried out twice to calculate the inspiratory capacity (IC) as the measured volume starting from the end of expiration to the total lung capacity (TLC) at 30 cmH$_2$O. We estimated the static compliance (Cstat) from these maneuvers. A 3-s multifrequency (1–20.5 Hz) volume perturbation was applied to the lungs for the measurement of respiratory input impedance from which we applied the constant phase model

and estimated: airway resistance (Rn), tissue damping (G) and tissue elastance (H). These parameters were measured initially after the injection of 20 µL/10 g body weight of phosphate-buffered saline (PBS), a diluent of MCh, by jugular vein and, then again after the following doses of MCh: 30, 100, 300, 1000 µg/kg in a volume of 20 µL/10 g body weight. In addition, hysteresivity (η) was calculated for the PBS dose. The data used were the peak response of each dose and expressed by the percentage increase over PBS.

Bronchoalveolar fluid (BALF)

At the end of the experiment, the lungs were washed twice with PBS (0.8 mL each wash). The BALF was centrifuged at 1,500 rpm, for 15 min. The supernatant was collected, and the pellet was resuspended in 1 mL of PBS. Total cell count (TCC) was made in a Neubauer chamber. For the differential cell analysis, BALF suspension was centrifuged in a cytospin and slides were stained with hematoxylin and eosin (NewProv, Brazil). Four hundred cells were counted under light microscopy. The total and differential counts were expressed by the number of cells $\times 10^5$ per mL of BALF.

Lung volume

After the BALF procedure, the lungs and trachea were removed from the animal, and through the 18G cannula, inserted into the trachea, the set was connected to a column, filled with 4% paraformaldehyde solution and the lungs were inflated under pressure of 25 cmH$_2$O for 15 min. After this procedure, the trachea was occluded and the volume of the lung was determined using Archimedes' Principle, which states that the buoyant force generated on a submerged body is quantitatively equal to the weight of the liquid displaced by the body itself. The data were expressed in milliliters (mL).

Morphological assessment

After measuring lung volume, the lungs remained in a 4% paraformaldehyde solution for 24 h and then were transferred to a 70% alcohol solution. Then, four tissue blocks per lung were prepared for paraffin embedding. The paraffin blocks were randomly cut (thickness at 5 µm) and stained with hematoxylin and eosin (HE). Images were digitally acquired employing an automated microscope (BioTek Lionheart FX, USA) at 20X and 10 images were randomly selected for further processing. Differences in lung parenchyma were evaluated by measuring the mean linear intercept (MLI). The MLI is a measure of the mean distance from the interalveolar septal wall, which is widely used to examine the size of the alveolar space. MLI was measured directly [18], with an automated digital method implemented (ImageJ 1.37, NIH, USA) and described elsewhere [6]. Collagen detection in the lung parenchyma was done by histological staining using Picrosirius Red. Only peripheral airways were considered for the assessment avoiding regions with blood vessels. The presence of collagen fibers was done by fluorescence microscopy (Zeiss Axioskop 2, Oberkochen, Germany) at 40X magnification employing an established method [50], and the area was digitally assessed (ImageJ 1.37, NIH, USA). The picrosirius positive area (PPA) was calculated as a percentage of the airway area.

Whole body plethysmography and respiratory chemoreflex analysis

The ventilatory response was assessed using whole-body plethysmography (EMKA Technologies, USA), on the same day, before the assessment of respiratory mechanics. The mice had prior contact with the plethysmography chambers for adaptation in the two days preceding the experiments. This way, we ensure that the change in environment does not interfere with ventilation measures. Briefly, conscious unrestrained freely moving mice were kept in a 0.5 L plethysmography chamber with room air for 45–60 min before starting to record the ventilatory parameters. Recording sessions were conducted between 9:00 am and 4:00 pm and lasted < 3 h. The plethysmography chamber was continuously flushed with 0.5 L/min, regulated by computer-driven mass flow controllers for O$_2$, N$_2$, and CO$_2$ (Alicat Scientific Inc., USA). SAMP8 or SAMR1 mice were exposed to different respiratory challenges, such as a) normoxia condition (FiO$_2$=0.21, balanced with N$_2$); b) normoxic hypercapnia (FiCO$_2$=0.07; FiO$_2$=0.21 and balanced N$_2$, for 10 min) and c) hypoxia (FiO$_2$=0.08, balanced with N$_2$, for 10 min). For the normoxic hypercapnia protocol, the inspired fraction of oxygen (FIO$_2$) stayed at the fraction of 0.21 during the whole protocol, similar to our previous studies [31]. After 10 min of normoxia, the inspired fraction of CO$_2$ (FiCO$_2$) increased from 0 to 0.07 and lasted 10 min, and then was followed by recovery in normoxia for at least 20 min. The hypoxia protocol was performed by exposing the mice to FiO$_2$=0.08 for 10 min, following a period of normoxia recovery (reoxygenation) for 20 min.

The ventilatory parameters measured by the plethysmography system were respiratory frequency (f$_R$, breaths/min), tidal volume (V$_T$, µL/g), and minute volume (V$_E$, µL/min/g; calculated as the product of f$_R$ x V$_T$), which were assess during periods free of movement artifacts. For the analysis of breathing during asleep (during the daytime), these variables were analyzed as the average of 120 s duration each. During normoxia, hypercapnia and hypoxia, the analysis of V$_T$, f$_R$, and V$_E$ were performed at 7–10 min from the beginning of the gas change.

To account for differences in body size, breath volumes were also normalized to body weight. Room temperature (23–26 °C) and humidity (50–60%) were continuously recorded inside the plethysmography chamber and used to calculate the tidal volume. Rectal temperature was used as a core body temperature index. The pressure signal was amplified, filtered, recorded, and analyzed offline using data acquisition/processing software (Powerlab 16/30, ML880/P, ADInstruments, NSW, Australia).

Brainstem histology

After the assessment of respiratory mechanics, mice were injected with heparin (500 units, intracardially) and perfused through the ascending aorta with 50 mL of PBS (pH 7.4) followed by 4% phosphate-buffered (0.1 M; pH 7.4) formaldehyde (Electron Microscopy Sciences, USA). The brainstem was removed and stored in the perfusion fixative for 24–48 h at 4 °C. Series of coronal Sects. (30 μm) from the brainstem were cut using a microtome and stored in cryoprotectant solution (20% glycerol plus 30% ethylene glycol in 50 mM phosphate buffer, pH 7.4) at -20 °C for up to 2 weeks awaiting histological processing. All histochemical procedures were done using free-floating sections according to previously described protocols [31].

The substance P receptor (NK1R) was detected using a rabbit NK1R antibody (1:5000 dilution; catalog#S8305; Sigma-Aldrich, USA) raised against a synthetic peptide corresponding to the C-terminal of NK1R of rat origin (amino acids 393–407). Biotinylated donkey anti-rabbit (1:500 dilution; catalog#717–067-003; Jackson Immunoresearch) followed by the ABC kit (Vector Laboratories Inc., Burlingame, USA) and subsequent colourization with 3,3′-diaminobenzidine (DAB). The specificity of the antibodies has been validated previously [31, 43]. All the sections were mounted onto slides in rostrocaudal sequential order, dried, and covered with DPX (Aldrich, Milwaukee, USA). Coverslips were affixed with nail polish.

Densitometric analysis of NK1R immunoreactivity

A conventional multifunction microscope (ZeissAxioskop A1, Germany) was used to image sections and perform subsequent analysis [25]. A one-in-four series of 30-μm-thick brainstem sections were used per animal, causing each section analyzed to be 120 μm apart. The sections were counted bilaterally, and the numbers reported in the results section correspond exactly to the counts of one-in-four sections in a series. Photographs were taken with a color camera (Zeiss AxiocamHRc, Germany). An image analysis software package (ImageJ 1.37, NIH, USA) was used for cell counting, and a technical illustration software package (Canvas, v.9.0; ACD Systems, USA) was used for line drawings, assembly

of figures and labelling. The neuroanatomical nomenclature used was defined by Franklin and Paxinos [9].

Images were taken through the region of interest from both sides of the entire ventral respiratory column using the same exposure time. The area of interest was outlined using the landmarks as follows. For the parafacial (pF) region, at bregma -6.36 mm, the area was defined by outlining from halfway down the medial edge of the facial motor nucleus, around the center of the ventral edge of this nucleus and then perpendicular to the ventral surface. The region continued medially along the ventral surface to the medial edge of the pyramidal tract and closed with a diagonal to the medial edge of the facial nucleus (see Figs. 2A-B). Note that the region of the medulla thus defined encompassed not only the parafacial but a large region medial to it. This choice was made because the parafacial per se is not identifiable in tissue reacted for standard NK1R immunochemistry because of the extremely low level of immunoreactivity [28, 43]. For the Bötzinger (BötzC) region, at bregma -6.64 mm, the region was defined by an oval 150 μm wide and 200 μm long, with the top centered on the ventral edge of the nucleus ambiguus (see Figs. 2C-D). For the Pre-Bötzinger (PreBötzC) region, at bregma -6.84 mm, the region was defined by an oval 150 μm wide and 200 μm long, with the top centered on the ventral edge of the nucleus ambiguus (see Figs. 2E-F). For the rostral ventral respiratory group (rVRG), at bregma -7.08 mm, the region was defined by an oval 150 μm wide and 200 μm long, with the top centered on the ventral edge of the nucleus ambiguus (see Figs. 2G-H). For the nucleus ambiguus (NA), at bregma -6.64; -6.84 and -7.08 mm, the region was defined by analyzing compact, semi-compact, and external formation, respectively.

The regions described above were digitally outlined (ImageJ 1.37, NIH, USA), and the region of interest was segmented such that the segments were judged to represent true immunostaining using the NA as a standard between sections. The area of pixels containing segments was calculated by the software, and the data are presented as a percentage of control values (SAMR1), with control as 100%.

Statistical analysis

The data analysis was performed with a statistics software (GraphPad Prism 7.01, GraphPad Software Inc., USA). Data were tested for normality using the Shapiro–Wilk test. Student's t test (MLI and collagen deposition), one-way (respiratory mechanics, and imunohistochemistry) or two-way (dose response curve to MCh, and ventilatory variables) ANOVA, usually with repeated measures, followed by Tukey's, Bonferroni's, or Holm-Sidak's multiple comparisons test. The F and p values for every effect and interaction between effects are reported in the figure legends or the results section. Differences were considered significant when

p < 0.05. In figures, data from each animal are presented in scatter plots, with summary data in text shown as mean ± SD unless noted otherwise.

Results

Body weight, NAL, lung volume and BALF

SAMP8 mice (10-month-old) had significantly lower body weight, naso-anal length (NAL) and lung volume compared to matched-age SAMR1 mice (Table 1). The total cell count, mononuclear and polynuclear cells in BALF did not differ between both strains (Table 1). Aging in SAMP8 mice significantly increased body at 10 months when compared to 3- and 6-month-old mice. No significant differences in NAL and lung volume were observed with aging. BALF counts showed a reduction in total and mononuclear cells at 10 months compared to young mice.

Breathing responses in unrestrained conscious mice.

The first series of experiments were performed to characterize baseline breathing patterns in 10-month-old unrestrained conscious SAMR1 and SAMP8 mice. We did not observe significant differences in baseline f_R (98.3 ± 11.6 vs. SAMR1 113.1 ± 11.1 breaths/min, p = 0.2, t = 1.3, df = 22, N = 9–14) and V_E (1835 ± 354 vs. SAMR1 1404.8 ± 418 μl/g/min, p = 0.15; t = 1.46, df = 22, N = 9–14) (Figs. 1A-B; 1D). However, baseline V_T showed a significant higher value in the SAMP8 animal model (19.75 ± 4.55 vs. SAMR1 12.47 ± 3.8 μl/g, p = 0.0074; t = 3.97, df = 21, N = 9–14) (Fig. 1C).

Challenging the animals to 8% O_2 (hypoxia ventilatory response—HVR), the increase in V_E (from 1835 ± 354 to 3793 ± 274 vs. SAMR1: from 1404.8 ± 418 to 3304 ± 231 μl/g/min, $F_{3,44} = 1.45$; p = 0.074) was not affected in SAMP8 mice (Figs. 1A-B). However, the tachypneic response to hypoxia was reduced (from 98.3 ± 11.6 to 193.2 ± 20.7 vs. SAMR1: from 113.1 ± 11.1 to 219.7 ± 6.1 breaths/min, $F_{3,44} = 141.9$; p = 0.001) in SAMP8 mice (Fig. 1D). We did not find significant differences in the increase in V_T ($F_{3,44} = 0.128$; p = 0.954) (Fig. 1C).

On the other hand, challenging the animals to 7% CO_2 (hypercapnia ventilatory response—HCVR), we found a significant further increase in V_T (from 19.2 ± 4.4 to 30 ± 3.2 vs. SAMR1: from 10.9 ± 2.6 to 17.3 ± 1.8 μl/g, $F_{3,34} = 120$; p = 0.0018) and V_E (from 1889 ± 364 to 6712 ± 1122 vs. SAMR1: from 1232 ± 303 to 4044 ± 440 μl/g/min, $F_{3,34} = 129.42$; p = 0.0015) in SAMP8 mice (Figs. 1A-C). The tachypneic response to hypercapnia (from 99.3 ± 12 to 143.6 ± 21.8 vs. SAMR1: from 112.5 ± 10.9 to 232.5 ± 26.5 breaths/min, $F_{3,34} = 95.87$; p = 0.02) was reduced in SAMP8 mice (Fig. 1D).

We did not find significant differences in body temperature during normoxic/normocapnic conditions in SAMR1 and SAMP8 (36.9 ± 0.1 vs. SAMR1 37.2 ± 0.1 ºC, p = 0.087). In addition, during the experiments, the mean chamber temperature was 25.3 ± 0.3 °C, and the mean room temperature was 24.8 ± 0.3 °C.

NK1r-expressing neurons in the brainstem in SAMR1 and SAMP8 mice.

Since breathing pattern was changed in SAMP8 mice, the following experiment was conducted to evaluate the ventral respiratory column in the ventral aspect of the brainstem. We observed a reduction of NK1-ir density in the rVRG ($71.7 \pm 1.8\%$ of the SAMR1, 28% reduction; p < 0.0001), PreBötC ($74.3 \pm 0.8\%$ of the SAMR1, 25.7% reduction; p < 0.0001), BötC ($68.2 \pm 4.3\%$ of the SAMR1, 31.6%

Table 1 Age, body weight, naso-anal length, lung volume, total cell count, mononuclear and polymorphonuclear cells of 3, 6, 10-old-month SAMP8 and 10-month-old SAMR1. Values are means ± SD. Significant differences among strains were analyzed by unpaired t-test. (*) Different from SAMR1; p < 0.05. Significant differences across ages were performed using One-way ANOVA and Tukey`s test for multiple comparisons. (†) Different from 10-month-old SAMP8; p < 0.05

Age	Body weight (g)	Naso-anal length (cm)	Lung volume (mL)	Total Count (× 10⁵ cells/mL)	Mononuclear (× 10⁵ cells/mL)	Polymorphonuclear (× 10⁵ cells/mL)
	$28.11 \pm 2.49^{\dagger}$ (n = 12)	9.36 ± 0.35 (n = 6)	1.28 ± 0.09 (n = 6)	$2.79 \pm 1.31^{\dagger}$ (n = 12)	$2.73 \pm 1.30^{\dagger}$ (n = 12)	$0.009 \pm 0.019^{\dagger}$ (n = 12)
	$29.86 \pm 2.29^{\dagger}$ (n = 15)	9.51 ± 0.26 (n = 8)	1.50 ± 0.26 (n = 7)	$2.72 \pm 1.43^{\dagger}$ (n = 14)	$2.70 \pm 1.35^{\dagger}$ (n = 14)	$0.004 \pm 0.006^{\dagger}$ (n = 14)
	$32.50 \pm 2.65^{*}$ (n = 16)	$9.54 \pm 0.32^{*}$ (n = 16)	$1.74 \pm 0.28^{*}$ (n = 13)	0.89 ± 0.71 (n = 25)	0.89 ± 0.15 (n = 25)	0.002 ± 0.001 (n = 25)
	44.31 ± 4.15 (n = 17)	11.03 ± 0.35 (n = 17)	2.32 ± 0.26 (n = 10)	0.99 ± 0.59 (n = 18)	0.98 ± 0.14 (n = 18)	0.002 ± 0.001 (n = 18)

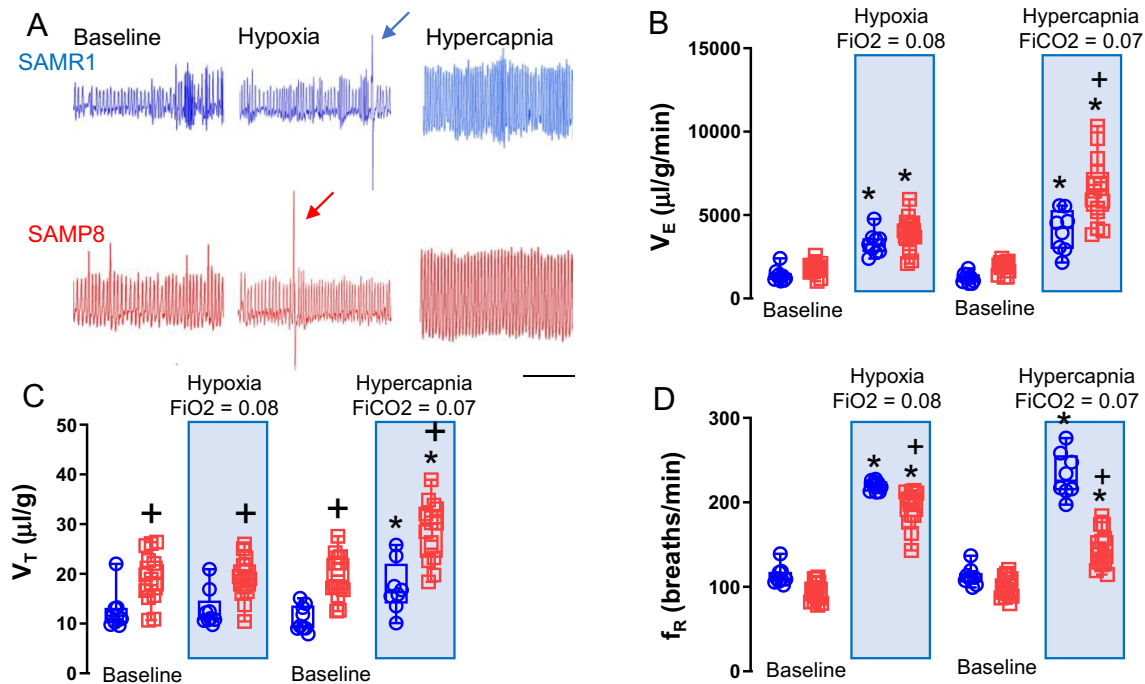**Fig. 1** Ventilatory responses in SAMR1 and SAMP8 mice

reduction; p = 0.0034) and pF region (71.1 ± 3.5% of the SAMR1, 28.9% reduction; p = 0.006) (Figs. 2A-I). We did not find a significant reduction in the density of NK1r neurons in the NA in all analyzed groups (95 ± 3.8% of the SAMR1, 5% reduction; p = 0.2171) (Fig. 2I).

Respiratory mechanics

The next step was to evaluate the properties of the lung analyzing the mechanics of breathing. First, we made a comparison of respiratory mechanics of SAMP8 mice at different ages (3, 6 and 10 months old). The time course showed an increase in static compliance (Cstat) ($F_{2,26}$ = 12.16; p = 0.0002) and inspiratory capacity (IC) ($F_{2,26}$ = 12.01; p = 0.0002) at 10-month-old (Figs. 3A-B). In addition, SAMP8 also showed a significant decrease in tissue resistance (R_n) ($F_{2,36}$ = 4.45; p = 0.018), tissue viscance (G) ($F_{2,36}$ = 12.36; p < 0.0001), and tissue elastance (H) ($F_{2,30}$ = 10.96; p = 0.0003) at 10-month-old (Figs. 3C-E). No significant change was observed on η ($F_{2,35}$ = 1.35; p = 0.27) (Fig. 3F).

To diagnose and assess the mechanisms of airway hyperresponsiveness we used the methacholine challenge (MCh: 30, 100, 300 and 1000 µg/kg). MCh (100, 300 and 1000 µg/kg) elicited a dose response increase of Rn ($F_{3,93}$ = 5.108.6; p = 0.0026), G ($F_{3,93}$ = 20.65; p < 0.0001), and H ($F_{3,93}$ = 5.014; p = 0.0029) both SAMR1 and SAMP8 mice (Figs. 4A-C). However, SAPM8 mice showed an attenuated increase in Rn ($F_{1,31}$ = 10.66; p = 0.0027), and G

($F_{1,31}$ = 24.90; p < 0.0001) reaching significant values at 300 and 1000 µg/kg (Figs. 4A-B). No significant difference was observed in the dose response curve of MCh in H analysis ($F_{1,31}$ = 0.37; p = 0.544) (Fig. 4C).

Morphological measurement

When we analyzed the MLI in lungs from SAMP8 and SAMR1 mice, we did not find a significant decrease in index of lung samples from SAMP8 animals (SAMP8 47.66 ± 2.79 µm vs. SAMR1 49.10 ± 3.45 µm) (t = 1.05, df = 8; p = 0.322) (Figs. 5A-C).

Collagen deposited around the airways was analyzed using Picrosirius staining. Notably, there was no differences in collagen deposition between the mouse strains (SAMP8: 83.98 ± 4.86% vs. SAMR1: 82.10 ± 2.99%) (t = 0.57, df = 6; p = 0.58) (Figs. 5D-F).

Discussion

This study demonstrates that a mouse model of accelerated aging (SAMP8) experiences ventilatory and lung dysfunctions. Considering SAMP8 mice show a myriad of aging-associated changes, including dementia and AD [21, 26, 33], we believe the present findings offer significant insights into the respiratory abnormalities associated with aging, and we hope that these insights can be leveraged to improve clinical
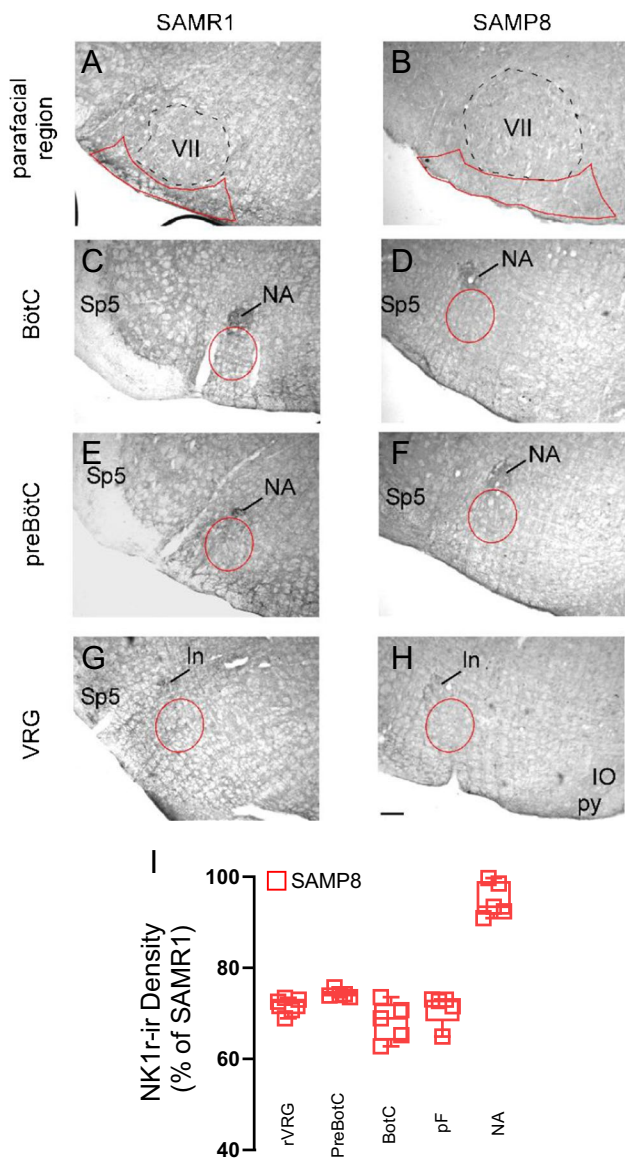
Fig. 2 Reduction of NK1 expression throughout the ventral respiratory column

Fig. 3 Respiratory mechanics parameters under static conditions at 3, 6, and 10-month-old SAMP8 mice

care for aged patients, especially with neurodegenerative diseases, in a near future.

Ventilatory impairment in SAMP8 mice

Breathing in mammals is controlled by a complex network of both excitatory and inhibitory neurons found in the ventrolateral medulla oblongata, specifically within an area known as the preBötzinger Complex (preBötC). This region is vital for the creation of various respiratory rhythms, such as normal breathing (eupnea), gasping, and sighing, as highlighted in prior research [15, 17, 53]. In our study, we observed a significant decrease in the expression of the NK1 receptor across several subnuclei of the ventral respiratory column,

including the respiratory parafacial region, the Bötzinger Complex (BötC), preBötC, and the rostral aspect of the ventral respiratory column (rVRG). While our findings do not conclusively show a decrease in neuron numbers throughout the ventral respiratory column, the diminished NK1 receptor expression is likely to have significant impacts on respiratory physiology. It is widely recognized that neurons in the parafacial region and the BötC/preBötC are crucial for driving breathing in mammals at rest. Evidence has consistently shown that the pharmacological or genetic removal of essential neurons within the ventral respiratory column impacts breathing during rest, as well as during quiet wakefulness and sleep [11]. In our current study using a genetic model of aging (SAMP8), we did not observe significant differences in resting respiratory output. This lack of change could be due to the fact that we observed less than a 30% reduction in NK1 expression in the ventral respiratory column. The fact that a high kill rate would be required to produce symptoms is expected. Parkinson's disease becomes symptomatic only with the loss of about 80% of the dopaminergic neurons [31]
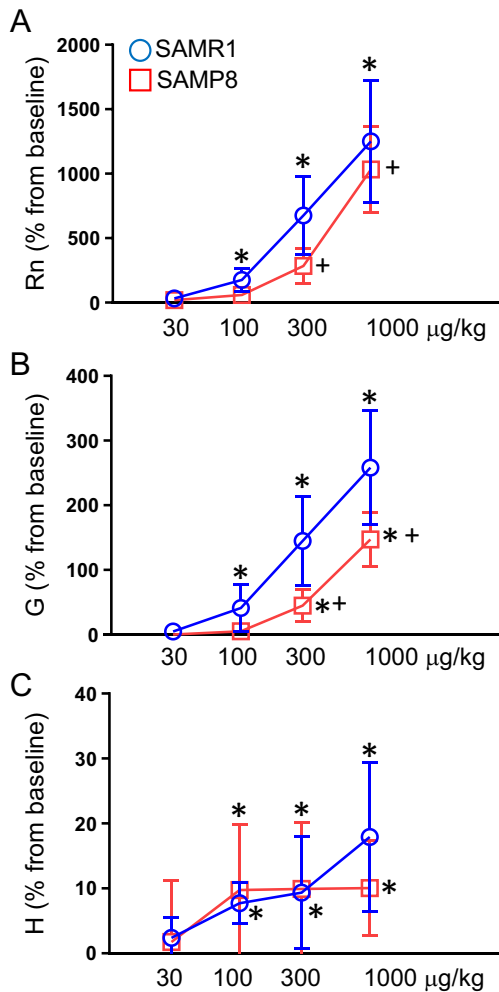
Fig. 4 Dose–response curves to methacholine (Mch) between 10-month-old SAMR1 mice and SAMP8

and the destruction of well over 80% of the C1 neurons is required to produce chronic hypotension and a cohort of associated autonomic deficits [23].

Central chemoreception involves the brain detecting differences in CO_2 and H^+ levels and their effects on breathing. In our study, we noted a 65% increase in the hypercapnic ventilatory response (HCVR) in SAMP8 animals, which was unexpected given the observed reduction in only 30% of the NK1 expression in ventral respiratory neurons. We did not assess other brain nuclei involved in respiratory regulation and chemosensation, which might explain the additional increase in HCVR. Therefore, further investigation is required to gain a clearer understanding of these findings. It is also possible that peripheral chemoreceptors, particularly the carotid body, might partly compensate for diminished central CO_2 sensitivity, although their role is inconsistently described in the literature [4, 8, 35, 43]. Peripheral chemoreceptors significantly activate the entire respiratory pattern generator and might

be essential for conveying the CO_2 response when central chemoreceptors are compromised [35, 43]. Furthermore, compensation by potential CO_2 sensing sites in the brain might either be inactive or lack sufficient connectivity to the respiratory pattern generator compared to control animals, as suggested by Nattie [27, 29].

In a streptozotocin-induced model of Alzheimer's disease (AD), an elevated HCVR was observed. This increased sensitivity to CO_2 was linked to significantly higher levels of amyloid-beta (Aβ) expression in the LC [49]. Although the hallmark pathological features of AD in this model, including neuroinflammation, oxidative stress, accumulation of phosphorylated tau and Aβ peptides, synaptic damage, and resultant behavioral changes underscore its value in translational research, discrepancies exist in the respiratory studies conducted so far. Therefore, the heightened hypercapnic response seen in SAMP8 mice may potentially be associated with the presence of Aβ in brain regions involved in CO_2 detection, such as the LC [49].

Research has been conducted to explore the potential relationship between AD and the hypoxia ventilatory response, given that changes in respiratory function could impact oxygen delivery to the brain. Some studies suggest that individuals with AD may experience changes in respiratory function, including changes in respiratory muscle strength and control. Yet, the specific mechanisms and extent of these modifications are still under investigation. In our current study, we observed a significant reduction in the tachypneic response to hypoxia or hypercapnia, likely due to impairment of neurons in the BötC/preBötC region, which are crucial for regulating breathing rhythm [1]. These rhythmogenic neurons are known to express NK1 receptors [11, 13].

A possible connection between accelerated aging and the hypoxia ventilatory response may involve the central nervous system, particularly the respiratory control centers. The degeneration of brain regions responsible for respiratory control could lead to altered breathing patterns, as shown in our SAMP8 model with a reduction in NK1 expression throughout the ventral respiratory column. Moreover, disruptions in the neural circuits that manage both cognitive and respiratory functions could influence the hypoxia ventilatory response in individuals with senescence. It is important to recognize that this field of research is continually evolving, and findings may vary across different studies. The relationship between aging and respiratory function is complex and likely multifactorial. Further research is essential to better understand the connections between neurodegenerative processes, respiratory function, and the hypoxic ventilatory response in aging, including those associated with aging itself.
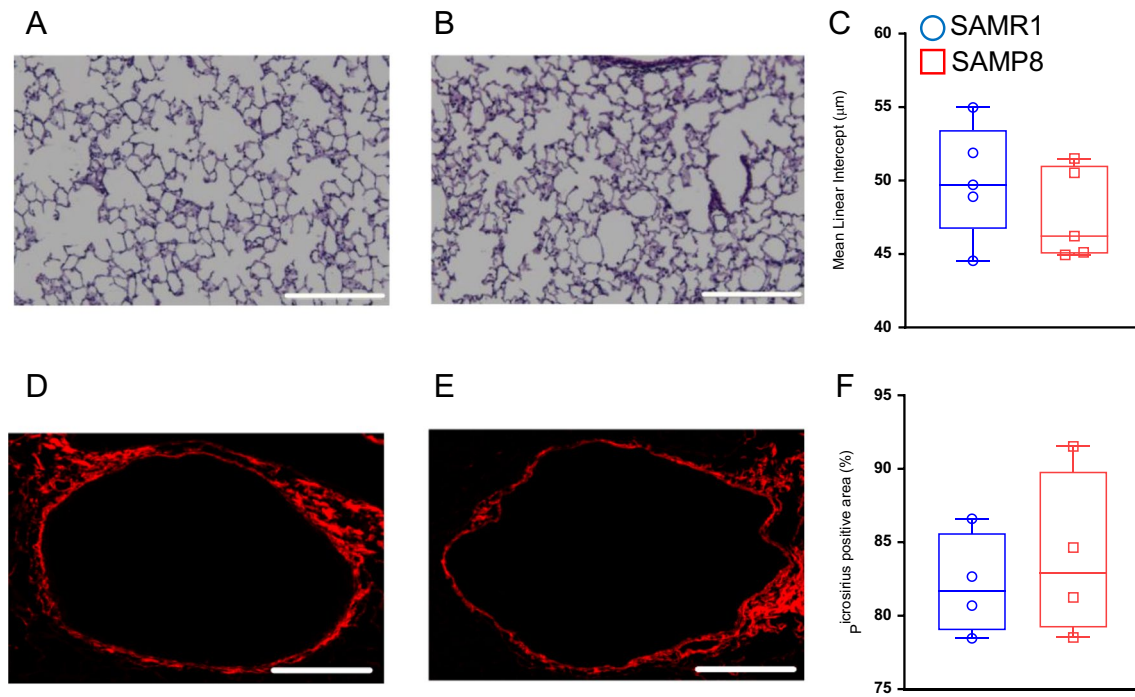
Fig. 5 Mean linear intercept and collagen deposition quantification

Respiratory mechanics and lung properties in SAMP8 mice

The literature suggested that changes in airways resistance and lung parenchyma vary in a nonlinear manner. Specifically, significant differences affect primarily the lung parenchyma and later the airways resistance. In a study with C57BL/6 J mice, R_n varied significantly from 20 to 26 months, but not from 2 to 20; the inverse situation happened with G and H [14]. In C57BL/B6 mice, the greatest change in R_n happened from 6 to 18 months whilst G and H changed significantly from 2 to 6 months [7]. Our findings evidenced that in SAMP8 mice the differences in airways resistance and lung parenchyma also did occur in a nonlinear manner. However, these differences in R_n, G, and H markedly happened only at 10 months (Fig. 3), suggesting that it might be a characteristic of these senescent animals.

Based on the existing experimental data documented in the literature, it appears that hysteresivity (η) exhibits a consistent value throughout the lifespan of mice but demonstrates an upward trend at later stages, particularly beyond 20 months [5, 14]. In lung pathologies affecting parenchyma, it is suggested that an increase in η coincides with the emergence of heterogeneities within the lung, which can be attributed to changes in the mechanical properties and behavior of biological tissues, particularly in their ability to deform and flow under stress [2]. Notably, variations in η have been observed in middle-aged

mice within emphysema models [48]. Although our findings did not indicate statistically significant differences in η, it is possible that the time course analyzed was not sufficient to observe any difference in η. However, with a longer period of analysis in the future, these changes could be explained by alterations in local airway resistance, as previously suggested [2]. Our inclination aligned with this proposition as the data of collagen deposition and MLI did not exhibit statistical differences between the SAMP8 experimental group and the control group.

Interestingly, we observed a significant reduction in contractile response to MCh doses of 300 and 1000 µg/kg in the SAMP8 mice when compared to the control group (Fig. 4). The literature suggests that differences in contractility between younger and older rats and rabbits may be attributed to variations in the quantity of airway smooth muscle or the availability of muscarinic receptors [20]. Conducting further studies to assess whether these differences in R_n result from mechanical interactions or physiological variations will help elucidate these findings.

Oscillometric studies conducted on humans have yielded conflicting results concerning the correlation between age and resistance [16]. While disparities exist, certain authors have suggested an age-related decline in resistance specifically among males [32]. Our observations in SAMP8 mice appeared to support these observations, although the precise underlying mechanisms were not explored in this study. Nonetheless, we hypothesized that the advancement of age

may lead to changes in peripheral lung function or the emergence of an airway shunt [40].

Regarding the lung parenchyma, we observed that 10-month-old SAMP8 mice suffered a reduction of elastance when compared to younger animals (3 and 6-month-old), showing emphysema-like characteristics, a feature of senescent mice that was pointed out in the literature [45, 47]. Several factors could potentially account for this phenomenon, including air space enlargement, changes in the extracellular matrix (ECM), or surfactant properties [39].

Limitations of the study

One limitation of this study is the absence of a control group for the progression of changes in respiratory mechanics. While SAMP8 mice were studied at 3, 6, and 10 months, the SAMR1 mice, which serve as a control group, were not included in this analysis. The absence of control group data currently limits our ability to make comprehensive comparisons and conclusions about the observed changes. However, we showed a consistent alteration in the respiratory mechanics of SAMP8 animals at 10 months of age, both in baseline and in response to methacholine. We recognize that future experiments will need to include the proper control group, SAMR1, to evaluate and compare the findings more effectively.

A second limitation of our study is the use of pancuronium bromide, a nicotinic acetylcholine receptor blocker. While the use of the neuromuscular blocker pancuronium is appropriate for procedures requiring mechanical ventilation [3], it is important to note that pancuronium bromide has a vagolytic effect that can influence airway caliber and pulmonary arterial pressure in a dose-dependent manner. This pharmacological effect may have affected some of our respiratory mechanics measurements. Despite using a fixed dose to ensure consistency, this remains a potential confounding factor.

Conclusions

In conclusion, the SAMP8 animal model of senescence exhibits a decreased tachypneic response to hypoxia and hypercapnia, along with a reduced contractile response to MCh compared to control animals. These findings suggest a failure in the respiratory mechanisms to adequately respond to challenges, which could significantly impact the physiology of breathing during senescence. Overall, these findings indicate that SAMP8 mice are a suitable model for researching the peripheral and central respiratory systems during the aging process and exploring how these aspects may be intertwined with AD-like characteristics in SAMP8 mice.

Whole body plethysmography was used to examine ventilation changes during exposure to hypoxia or to hypercapnia. A) Plethysmography recordings of a SAMR1 (blue) and SAMP8 (red) mice under baseline, hypoxia or hypercapnia conditions. Changes in B) ventilation (VE, µl/g/min), C) tidal volume (VT, µl/g), and D) respiratory rate (fR, bpm) in control (SAMR1—blue) and SAMP8 (red) animals exposed to hypoxia ($FiO_2 = 0.08$) or hypercapnia ($FiCO_2 = 0.07$. Arrows indicate the sigh in both SAMR1 and SAMP8 under hypoxia. *Different from baseline; + different from SAMR1; Two-Way ANOVA followed by Sidak's multiple comparisons tests; $p < 0.05$; N = 10–15/group of mice. Scale bar in A = 5 s.

Representative photomicrographs of SAMR1 (control; A, C, E, and G) and SAMP8 (B, D, F, and H) showing immunoreactivity for NK1 receptors in the respiratory parafacial region (pF) (A and B), Bötzinger complex (BötC) (C and D), pre-Bötzinger complex (preBötC) (E and F), and rostral ventral respiratory group (rVRG) (G and H). Analysis of the extent of NK1R immunoreactivity in the regions outlined by the red line in A-H. The NK1R immunoreactivity is expressed as a percentage of the immunoreactivity in the control (SAMR1) group. Abbreviations: IO, inferior olive, ln, nucleus linearis; NA, nucleus ambigus; py, pyramide; Sp5, spinal trigeminal nucleus, and VII, facial motor nucleus. Scale bar in H represents 200 µm and applies to A to H.

A) Static compliance (C_{stat}, cmH$_2$0/mL), B) inspiratory capacity (IC, mL), C) airway resistance (R_n, cmH$_2$0.s/mL), D) tissue viscance (G, cmH$_2$0/mL), E) tissue elastance (H, cmH$_2$0/mL), and F) hysteresivity (η) in SAMP8 mice at 3 (N = 12); 6 (N = 15) and 10-month-old (N = 16). The results are expressed as mean ± SD. * Different from 3-month-old mice. Significant differences ($p < 0.05$) were determined using One-way ANOVA and Tukey`s test for multiple comparisons.

A) airway resistance (R_n, cmH$_2$0.s/mL), B) tissue viscance (G, cmH$_2$0/mL), C) tissue elastance (H, cmH$_2$0/mL) in 10-month-old SAMR1 (N = 17), and SAMP8 mice (N = 16) during intravenous infusion of MCh (30, 100, 300 and 1000 µg/kg). Values are presented as the increased percentage from the basaline measurement. The results are expressed as mean ± SD. Significant differences were analyzed by Two-way ANOVA followed by Sidak's multiple comparisons tests ($p < 0.05$). * Different from baseline; + Different from SAMR1 (dose comparison).

A and B) Sections from lung parenchyma were stained with hematoxylin and eosin of 10-month-old SAMR1 (A) and SAMP8 (B) mice. C) Mean linear intercept in SAMR1 and SAMP8 mice (N = 4–5/group). D) Peripheral airways were stained with Picrosirius Red of 10-month-old SAMR1 (D) and SAMP8 (E) mice. Magnification at 40x. F) Collagen deposition in SAMR1 and SAMP8 mice (N = 4–5/

group). Scale bar in A and B = 200 μm; scale bar in D and E = 20 μm.

Declarations

References

1. Baertsch NA, Baertsch HC, Ramirez JM (2018) The interdependence of excitation and inhibition for the control of dynamic breathing rhythms. Nat Commun 9. https://doi.org/10.1038/s41467-018-03223-x

2. Bates JH, Lutchen KR (2005) The interface between measurement and modeling of peripheral lung mechanics. Respir Physiol Neurobiol 148(1–2):153–164. https://doi.org/10.1016/j.resp.2005.04.021

3. Bates JHT, Irvin CG (2003) Measuring lung function in mice: The phenotyping uncertainty principle. J Appl Physiol 94(4):1297–306

4. Blain GM, Smith CA, Henderson KS, Dempsey JA (2009) Contribution of the carotid body chemoreceptors to eupneic ventilation in the intact, unanesthetized dog. J Appl Physiol 106. https://doi.org/10.1152/japplphysiol.91590.2008

5. Bozanich EM, Collins RA, Thamrin C, Hantos Z, Sly PD, Turner DJ (2005) Developmental changes in airway and tissue mechanics in mice. J Appl Physiol 99. https://doi.org/10.1152/japplphysiol.01111.2004

6. Crowley G, Kwon S, Caraher EJ, Haider SH, Lam R, Batra P, Melles D, Liu M, Nolan A (2019) Quantitative lung morphology: Semi-automated measurement of mean linear intercept. BMC Pulm Med 19. https://doi.org/10.1186/s12890-019-0915-6

7. Elliott JE, Mantilla CB, Pabelick CM, Roden AC, Sieck GC (2016) Aging-related changes in respiratory system mechanics and morphometry in mice. Am J Physiol Lung Cell Mol Physiol 311. https://doi.org/10.1152/ajplung.00232.2016

8. Forster H V., Pan LG, Lowry TF, Serra A, Wenninger J, Martino P (2000) Important role of carotid chemoreceptor afferents in control of breathing of adult and neonatal mammals. In: Respiration Physiology

9. Paxinos G, Franklin KBJ (2001) The mouse brain in stereotaxic coordinates, 2nd 711 Edition. Academic Press, San Diego

10. Gaugler J, James B, Johnson T, Scholz K, Weuve J (2016) 2016 Alzheimer's disease facts and figures. Alzheimer's and Dementia 12. https://doi.org/10.1016/j.jalz.2016.03.001

11. Gray PA, Janczewski WA, Mellen N, McCrimmon DR, Feldman JL (2001) Normal breathing requires preBötzinger complex neurokinin-1 receptor-expressing neurons. Nat Neurosci 4:927–930. https://doi.org/10.1038/nn0901-927

12. Griñán-Ferré C, Corpas R, Puigoriol-Illamola D, Palomera-Ávalos V, Sanfeliu C, Pallàs M (2018) Understanding Epigenetics in the Neurodegeneration of Alzheimer's Disease: SAMP8 Mouse Model. J Alzheimer's Dis 62(3):943–63

13. Guyenet PG, Wang H (2001) Pre-Bötzinger neurons with preinspiratory discharges "in vivo" express NK1 receptors in the rat. J Neurophysiol 86. https://doi.org/10.1152/jn.2001.86.1.438

14. Huang K, Rabold R, Schofield B, Mitzner W, Tankersley CG (2007) Age-dependent changes of airway and lung parenchyma in C57BL/6J mice. J Appl Physiol 102. https://doi.org/10.1152/japplphysiol.00400.2006

15. Janczewski WA, Tashima A, Hsu P, Cui Y, Feldman JL (2013) Role of inhibition in respiratory pattern generation. J Neurosci 33. https://doi.org/10.1523/JNEUROSCI.1595-12.2013

16. Kalchiem-Dekel O, Hines SE (2018) Forty years of reference values for respiratory system impedance in adults: 1977–2017. Respir Med 136:37–47

17. Kam K, Worrell JW, Ventalon C, Emiliani V, Feldman JL (2013) Emergence of population bursts from simultaneous activation of small subsets of preBötzinger complex inspiratory neurons. J Neurosci 33. https://doi.org/10.1523/JNEUROSCI.4574-12.2013

18. Knudsen L, Weibel ER, Gundersen HJG, Weinstein F V., Ochs M (2010) Assessment of air space size characteristics by intercept (chord) measurement: An accurate and efficient stereological approach. J Appl Physiol 108. https://doi.org/10.1152/japplphysiol.01100.2009

19. Kõks S, Dogan S, Tuna BG, González-Navarro H, Potter P, Vandenbroucke RE (2016) Mouse models of ageing and their relevance to disease. Mech Ageing Dev 160:41–53

20. Lee HK, Lim MY, Bok SM, Cho ES, Lee EM, Kim SW, Kim YH, Kim HW (2007) Age differences in cholinergic airway responsiveness in relation with muscarinic receptor subtypes. Life Sci 81. https://doi.org/10.1016/j.lfs.2007.05.002

21. Liu B, Liu J, Shi JS (2020) SAMP8 Mice as a Model of Age-Related Cognition Decline with Underlying Mechanisms in Alzheimer's Disease. J Alzheimer's Dis 75(2):385–95

22. Lutsey PL, Chen N, Mirabelli MC, Lakshminarayan K, Knopman DS, Vossel KA, Gottesman RF, Mosley TH, Alonso A (2019) Impaired lung function, lung disease, and risk of incident dementia. Am J Respir Crit Care Med 199. https://doi.org/10.1164/rccm.201807-1220OC

23. Madden CJ, Stocker SD, Sved AF (2006) Attenuation of homeostatic responses to hypotension and glucoprivation after destruction of catecholaminergic rostral ventrolateral medulla neurons. Am J Physiol Regul Integr Comp Physiol 291. https://doi.org/10.1152/ajpregu.00800.2005

24. Marie A, Larroze-Chicot P, Cosnier-Pucheu S, Gonzalez-Gonzalez S (2017) Senescence-accelerated mouse prone 8 (SAMP8) as a model of age-related hearing loss. Neurosci Lett 656. https://doi.org/10.1016/j.neulet.2017.07.037

25. Miranda NC, Oliveira LM, Aquino YC, Moreira TS, Takakura AC (2023) The Pedunculopontine Tegmental Nucleus is not Important for Breathing Impairments Observed in a Parkinson's Disease Model. Neuroscience 512. https://doi.org/10.1016/j.neuroscience.2022.12.022

26. Morley JE, Armbrecht HJ, Farr SA, Kumar VB (2012) The senescence accelerated mouse (SAMP8) as a model for oxidative stress and Alzheimer's disease. Biochim Biophys Acta Mol Basis Dis 1822. https://doi.org/10.1016/j.bbadis.2011.11.015

27. Nattie E (2011) Julius H. Comroe, Jr., Distinguished lecture: Central chemoreception: Then ...and now. J Appl Physiol 110 (1):1-8

28. Nattie EE, Li A (2002) Substance P-saporin lesion of neurons with NK1 receptors in one chemoreceptor site in rats decreases ventilation and chemosensitivity. Journal of Physiology 544. https://doi.org/10.1113/jphysiol.2002.020032

29. Nattie E, Li A (2009) Central chemoreception is a complex system function that involves multiple brain stem sites. J Appl Physiol 106(4):1464–6

30. Nomura Y, Okuma Y (1999) Age-related defects in lifespan and learning ability in SAMP8 mice. Neurobiol Aging 20. https://doi.org/10.1016/S0197-4580(99)00006-8

31. Oliveira LM, Oliveira MA, Moriya HT, Moreira TS, Takakura AC (2019) Respiratory disturbances in a mouse model of Parkinson's disease. Exp Physiol 104. https://doi.org/10.1113/EP087507

32. Oostveen E, Boda K, Van Der Grinten CPM, James AL, Young S, Nieland H, Hantos Z (2013) Respiratory impedance in healthy subjects: Baseline values and bronchodilator response. European Respiratory Journal 42. https://doi.org/10.1183/09031936.00126212

33. Pallas M, Camins A, Smith MA, Perry G, Lee HG, Casadesus G (2008) From aging to Alzheimer's disease: Unveiling "The switch" with the senescence-accelerated mouse model (SAMP8). J Alzheimer's Dis 15(4):615–24

34. Poon HF, Farr SA, Thongboonkerd V, Lynn BC, Banks WA, Morley JE, Klein JB, Butterfield DA (2005) Proteomic analysis of specific brain proteins in aged SAMP8 mice treated with alpha-lipoic acid: Implications for aging and age-related neurodegenerative disorders. Neurochem Int 46. https://doi.org/10.1016/j.neuint.2004.07.008

35. Ramanantsoa N, Hirsch MR, Thoby-Brisson M, Dubreuil V, Bouvier J, Ruffault PL, Matrot B, Fortin G, Brunet JF, Gallego J, Goridis C (2011) Breathing without Co2 chemosensitivity in conditional Phox2b mutants. J Neurosci 31. https://doi.org/10.1523/JNEUROSCI.1721-11.2011

36. Reynolds CF, Kupfer DJ, Taska LS, Hoch CC, Sewitch DE, Restifo K, Spiker DG, Zimmer B, Marin RS, Nelson J (1985) Sleep apnea in Alzheimer's dementia: Correlation with mental deterioration. J Clin Psychiatry 46(7):257–61

37. Sanches VS, Santos FM, Fernandes JM, Santos MLM, Müller PT, Christofoletti G (2014) Neurodegenerative disorders increase decline in respiratory muscle strength in older adults. Respir Care 59. https://doi.org/10.4187/respcare.03063

38. Sastre M, Klockgether T, Heneka MT (2006) Contribution of inflammatory processes to Alzheimer's disease: Molecular mechanisms. Int J Dev Neurosci 24(2–3):167–76

39. Schulte H, Mühlfeld C, Brandenberger C (2019) Age-Related Structural and Functional Changes in the Mouse Lung. Front Physiol 10. https://doi.org/10.3389/fphys.2019.01466

40. Schulz H, Flexeder C, Behr J, Heier M, Holle R, Huber RM, Jörres RA, Nowak D, Peters A, Wichmann HE, Heinrich J, Karrasch S (2013) Reference Values of Impulse Oscillometric Lung Function Indices in Adults of Advanced Age. PLoS One 8. https://doi.org/10.1371/journal.pone.0063366

41. Sreedhar R, Giridharan V V., Arumugam S, Karuppagounder V, Palaniyandi SS, Krishnamurthy P, Quevedo J, Watanabe K, Konishi T, Thandavarayan RA (2016) Role of MAPK-mediated endoplasmic reticulum stress signaling in the heart during aging in senescence-accelerated prone mice. BioFactors 42. https://doi.org/10.1002/biof.1280

42. Sureda A, Capó X, Tejada S (2017) Neuroprotective Effects of Flavonoid Compounds on Neuronal Death Associated to Alzheimer's Disease. Curr Med Chem 26. https://doi.org/10.2174/0929867325666171226103237

43. Takakura AC, Barna BF, Cruz JC, Colombari E, Moreira TS (2014) Phox2b-expressing retrotrapezoid neurons and the integration of central and peripheral chemosensory control of breathing in conscious rats. Exp Physiol 99. https://doi.org/10.1113/expphysiol.2013.076752

44. Takeda T, Hosokawa M, Takeshita S, Irino M, Higuchi K, Matsushita T, Tomita Y, Yasuhira K, Hamamoto H, Shimizu K, Ishii M, Yamamuro T (1981) A new murine model of accelerated senescence. Mech Ageing Dev 17. https://doi.org/10.1016/0047-6374(81)90084-1

45. Takeda T, Hosokawa M, Higuchi K, Hosono M, Akiguchi I, Katoh H (1994) A novel murine model of aging, Senescence-Accelerated Mouse (SAM). Arch Gerontol Geriat 19. https://doi.org/10.1016/0167-4943(94)90039-6

46. Tomobe K, Nomura Y (2009) Neurochemistry, neuropathology, and heredity in samp8: A mouse model of senescence. Neurochem Res 34:660–9

47. Uejima Y, Fukuchi Y, Nagase T, Tabata R, Orimo H (1991) A new murine model of aging lung: The senescence accelerated mouse (SAM)-P. Mech Ageing Dev 61. https://doi.org/10.1016/0047-6374(91)90057-7

48. Vanoirbeek JAJ, Rinaldi M, De Vooght V, Haenen S, Bobic S, Gayan-Ramirez G, Hoet PHM, Verbeken E, Decramer M, Nemery B, Janssens W (2010) Noninvasive and invasive pulmonary function in mouse models of obstructive and restrictive respiratory diseases. Am J Respir Cell Mol Biol 42. https://doi.org/10.1165/rcmb.2008-0487OC

49. Vicente MC, Almeida MC, Bícego KC, Carrettiero DC, Gargaglioni LH (2018) Hypercapnic and Hypoxic Respiratory Response during Wakefulness and Sleep in a Streptozotocin Model of Alzheimer's Disease in Rats. Journal of Alzheimer's Disease 65. https://doi.org/10.3233/JAD-180397

50. Vogel B, Siebert H, Hofmann U, Frantz S (2015) Determination of collagen content within picrosirius red stained paraffin-embedded tissue sections using fluorescence microscopy. MethodsX 2. https://doi.org/10.1016/j.mex.2015.02.007

51. Wang J, Dove A, Song R, Qi X, Ma J, Bennett DA, Xu W (2022) Poor pulmonary function is associated with mild cognitive impairment, its progression to dementia, and brain pathologies: A community-based cohort study. Alzheimer's and Dementia 18. https://doi.org/10.1002/alz.12625

52. Wei X, Zhang Y, Zhou J (1999) Alzheimer's disease-related gene expression in the brain of senescence accelerated mouse. Neurosci Lett 268. https://doi.org/10.1016/S0304-3940(99)00396-1

53. Zanella S, Doi A, Garcia AJ, Elsen F, Kirsch S, Wei AD, Ramirez JM (2014) When norepinephrine becomes a driver of breathing irregularities: How intermittent hypoxia fundamentally alters the modulatory response of the respiratory network. Journal of Neuroscience 34. https://doi.org/10.1523/JNEUROSCI.3644-12.2014

54. Zeng Y, Wang PH, Zhang M, Du JR (2016) Aging-related renal injury and inflammation are associated with downregulation of Klotho and induction of RIG-I/NF-κB signaling pathway in senescence-accelerated mice. Aging Clin Exp Res 28. https://doi.org/10.1007/s40520-015-0371-y